RESEARCH ARTICLE

Editor's Choice

ADVANCED MATERIALS
www.advmat.de

Glucose-Triggered Gelation of Supramolecular Peptide Nanocoils with Glucose-Binding Motifs

*Sihan Yu, Zhou Ye, Rajdip Roy, Ravi R. Sonani, Irawan Pramudya, Sijie Xian, Yuanhui Xiang, Guoqiang Liu, Belen Flores, Einat Nativ-Roth, Ronit Bitton, Edward H. Egelman, and Matthew J. Webber**

Peptide self-assembly is a powerful tool to prepare functional materials at the nanoscale. Often, the resulting materials have high aspect-ratio, with intermolecular β-sheet formation underlying 1D fibrillar structures. Inspired by dynamic structures in nature, peptide self-assembly is increasingly moving toward stimuli-responsive designs wherein assembled structures are formed, altered, or dissipated in response to a specific cue. Here, a peptide bearing a prosthetic glucose-binding phenylboronic acid (PBA) is demonstrated to self-assemble into an uncommon nanocoil morphology. These nanocoils arise from antiparallel β-sheets, with molecules aligned parallel to the long axis of the coil. The binding of glucose to the PBA motif stabilizes and elongates the nanocoil, driving entanglement and gelation at physiological glucose levels. The glucose-dependent gelation of these materials is then explored for the encapsulation and release of a therapeutic agent, glucagon, that corrects low blood glucose levels. Accordingly, the release of glucagon from the nanocoil hydrogels is inversely related to glucose level. When evaluated in a mouse model of severe acute hypoglycemia, glucagon delivered from glucose-stabilized nanocoil hydrogels demonstrates increased protection compared to delivery of the agent alone or within a control nanocoil hydrogel that is not stabilized by glucose.

1. Introduction

Molecular constituents designed for self-assembly offer a powerful and thermodynamically driven route to achieve nanoscale order and recreate elegant and organized structures found in the living world.[1] Proteins are key building blocks underlying self-assembly of many natural materials.[2] The presence of certain analytes in the physiologic milieu can regulate the state and/or stability of biological matter arising from noncovalent filamentous protein assemblies, as seen in cytoskeletal actin and microtubules.[3,4] These natural materials have inspired the design of synthetic analogues of small molecule, protein, or colloidal assemblies that form explicitly from the binding and/or chemical reaction of small analyte molecules (e.g., ATP).[5–8] Accordingly, dynamic, reversible, and/or nonequilibrium assemblies arising from the binding or consumption of small molecule triggers have been demonstrated.[9] Peptides, in particular, are a useful platform from which to design self-assembling nanomaterials,[10–13] with some designs integrating functionality to further modulate the formation or properties of these assemblies in response to a specific trigger.[14–19]

In the context of analytes found in the human body, glucose is of particular interest; though ubiquitous, poorly controlled glucose levels are a symptomatic hallmark of diabetes. Numerous glucose-responsive material platforms have been designed by leveraging synthetic or protein-derived glucose-binding motifs in order to better treat diabetes.[20,21] Other related works have used enzymatic conversion of glucose by glucose oxidase (GOx) to actuate pH-dependent material outcomes. The self-assembly of a peptide gelator was designed to be governed by continuous conversion of glucose using GOx, with the material dissipating under conditions of low glucose to release glucagon, a therapeutic remedy for low blood glucose levels.[22] The gelation of this material, driven by the presence of glucose, offered opposing function to most glucose-responsive materials reported thus far, which typically de-gel, swell, or dissipate under conditions of high glucose to release insulin.[20,21]

S. Yu, Z. Ye, R. Roy, I. Pramudya, S. Xian, Y. Xiang, B. Flores, M. J. Webber
Department of Chemical & Biomolecular Engineering
University of Notre Dame
105 McCourtney Hall, Notre Dame IN 46556, USA
E-mail: mwebber@nd.edu

R. R. Sonani, E. H. Egelman
Department of Biochemistry and Molecular Genetics
University of Virginia
Charlottesville VA 22903, USA

G. Liu
Integrated Biomedical Sciences Program
University of Notre Dame
Notre Dame IN 46556, USA

E. Nativ-Roth, R. Bitton
Department of Chemical Engineering
Ben-Gurion University of the Negev
Beer-Sheva 84105, Israel

The ORCID identification number(s) for the author(s) of this article can be found under https://doi.org/10.1002/adma.202311498

DOI: 10.1002/adma.202311498

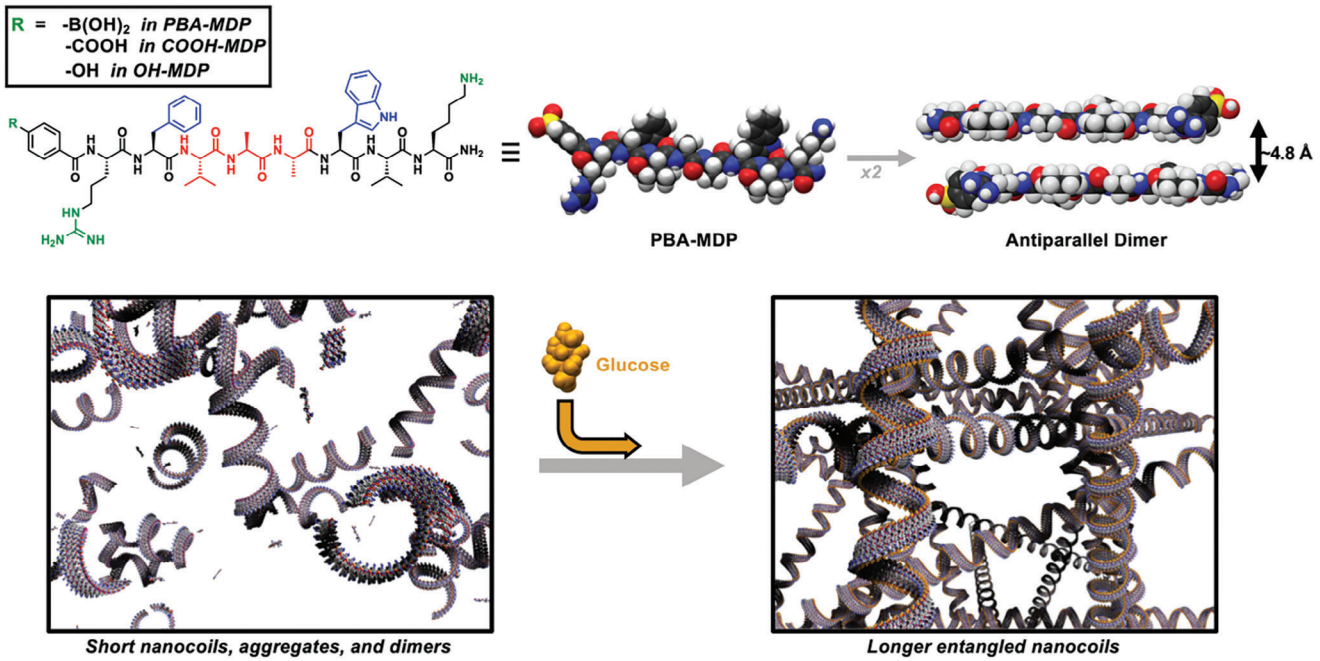

Figure 1. The chemical structure of PBA-MDP and control molecules (COOH-MDP and OH-MDP) used in this study (top) which demonstrate a preference for antiparallel dimer formation. PBA-MDP contains phenylboronic acid (PBA) which is Lewis acid capable of forming a charged tetrahedral boronate through dynamic-covalent interactions with glucose. Short nanocoils arise from PBA-MDP self-assembly, and upon addition of glucose (orange) these nanocoils elongate and entangle (bottom).

However, the use of a xenogeneic GOx enzyme to achieve glucose analyte-dependent self-assembly has attendant complications related to its immunogenicity along with toxic hydrogen peroxide byproducts that result from its conversion of glucose to gluconic acid.[21]

As a synthetic alternative to enzymatic modes of glucose sensing, phenylboronic acid (PBA) motifs are often used.[23,24] PBAs are Lewis acids that are capable of dynamic-covalent bonding to *cis*-1,2 and *cis*-1,3 diols when pH is at or above their p*K*a, stabilizing the negatively charged tetrahedral boronate.[25] As glucose is a *cis*-1,2 diol, its binding therefore increases the overall charge state of the PBA motif, a feature often used to introduce electrostatic repulsion or swelling in a material for glucose-responsive release of insulin.[21] Importantly, however, PBA motifs are not specific for glucose binding and are able to bind to many other *cis*-diol molecules found in the normal physiological environment, and in many cases bind to these better than to glucose.[23,26] Herein, a multidomain peptide (MDP) bearing a terminal PBA motif (PBA-MDP) is reported to assemble through antiparallel stacking into an uncommon nanocoil morphology (**Figure 1**). Upon addition of glucose, preexisting short nanocoils elongate and entangle to form self-supporting hydrogels. The hydrogels can encapsulate glucagon, with its controlled release inversely related to the bulk glucose concentration. When explored in an animal model of acute hypoglycemia, prophylactic injection of glucagon-loaded PBA-MDP hydrogels offers protection against severe outcomes and more rapid blood glucose recovery. Accordingly, the glucose-triggered entanglement and gelation of PBA-MDP nanocoils provides a synthetic and enzyme-free route to link material form to glucose level.

2. Results and Discussion

2.1. Multidomain Peptide Design

The general design of the PBA-MDP molecule (Figure 1; and Figure S1, Supporting Information) consisted of eight amino acid residues functionalized with a PBA motif at the *N*-terminus (PBA-RFVAAWVK). This design was inspired by prior reports of MDPs that note a criteria of ABA oligopeptide patterning, wherein two charged/hydrophilic "A" blocks flank a hydrophobic "B" block.[27] However, in addition to the inclusion of the prosthetic PBA motif, the design here differed from typical MDP designs by having only a single cationic amino acid for the "A" blocks, and also broke from the typical approach in its asymmetric sequence. The design rationale for each component was as follows: i) cationic residues at the N- and C-terminal ends consisting of an arginine (R) and lysine (K), respectively, serve as charge-bearing units and enhance solubility; ii) a hydrophobic "B" segment that included aromatic phenylalanine (F) and tryptophan (W) residues shielding an internal β-sheet forming region of valine (V) and alanine (A) residues; and iii) a glucose-binding PBA motif intended to shift the net charge on the N-terminal domain of the PBA-MDP as a function of glucose level. The particular amide-linked PBA motif chosen would be expected to have a pK_a of ≈8.4 on its own.[23] While this would not typically be effective for glucose-binding function under conditions of physiological pH, its positioning next to the cationic arginine residue was envisioned to significantly reduce its effective pK_a, a phenomenon also observed in PBA-modified cationic polymers.[28]

In addition to PBA-MDP, two control molecules were prepared to capture the general structure and range of charge states of

the prosthetic PBA motif. The first (COOH-MDP) was designed with a benzoic acid group in place of the boronate (Figure 1; and Figure S2, Supporting Information). The pK_a of this benzoic acid group is expected to be ≈4,[29] meaning it would be fully charged at neutral pH conditions used in these experiments. The second (OH-MDP) was designed with a phenol group in place of the boronate (Figure 1; and Figure S3, Supporting Information). As the pK_a of this phenol is expected to be ≈10, the motif should be uncharged at neutral pH conditions used in these experiments. It is possible that proximity to arginine could likewise shift pK_a of the phenol, as postulated for the PBA motif. It is also important to note that the expected pK_a of amino acids and prosthetic motifs used to construct all of the MDPs here could shift as a result of their position on the peptide and/or due to aggregation-induced pK_a shifts.[30,31] Efforts to quantify pK_a values for the various ionizable groups in these peptides via titration did not yield precise measurements and instead suggested a range of charged states, likely due to a broadened charge distribution resulting from peptide assembly.

2.2. Nanocoil Assembly

Given the design rationale for PBA-MDP, it was of interest to first study its propensity for self-assembly into nanostructures, as is commonly observed for other classes of MDPs and related oligopeptide motifs. When samples at 0.2% w/v were examined using cryogenic transmission electron microscopy (cryoTEM), the PBA-MDP was observed to self-assemble into relatively short and small nanocoils (**Figure 2**A). This nanocoil structure, resembling a telephone cord, is uncommon in MDPs and related oligopeptide assemblies formed from β-sheet segments, which instead more commonly form high aspect-ratio cylindrical micelles or ribbon-like filaments. To our knowledge, the formation of nanocoils of this type has only been observed from the self-assembly of tetrapeptides functionalized at both termini with S-aroylthiooximes for use as H_2S donors.[32–34] Upon addition of glucose at a concentration of 100 mg dL^{-1}, recreating normal glucose levels in the human body, the nanocoil structures were retained though appeared longer with a higher extent of nanostructure bundling (Figure 2B). The lengths of nanocoils in these two states were quantified by measuring every particle visible in four separate cryoTEM images collected from each glucose condition, revealing lengths in the case of PBA-MDP prepared at 100 mg dL^{-1} glucose (122 ± 63 nm, mean ± SD) that were significantly longer (P <0.0001, Student's t-test) than in 0 mg dL^{-1} glucose (77 ± 46 nm). Apart from differences in length, the nanocoil morphology was consistent over a range of different glucose levels (Figure S4, Supporting Information). Solution-phase AFM was also performed (Figure 2C), revealing nanocoil structures with features matching those seen by cryoTEM. TEM analysis of the control molecules showed nanocoils for the COOH-MDP molecule (length of 127 ± 45 nm from cryoTEM images) that were similar to those observed for PBA-MDP (Figure S5, Supporting Information), while OH-MDP formed anomalous small aggregates (Figure S6, Supporting Information). Accordingly, the formation of nanocoils seemingly depends on the availability of a negative charge at the position where the PBA has been inserted, thereby rendering the N-terminal end of the molecule effectively neutral. This data from the two control MDPs also suggests that the boronates on PBA-MDP are at least partially in their negatively charged conformation even in the absence of glucose, confirming expectations that the adjacent arginine residue reduces the effective pK_a of the boronate.

These structures were further characterized using small angle X-ray scattering (SAXS) (Figure 2D), with data fit to a model of spherical objects packed into a helical structure.[35] This is the same model used to analyze SAXS data from the only other reported peptide-based nanocoil assembly.[32] In the absence of glucose, PBA-MDP nanocoils had a coil diameter of 47 Å with a helical pitch of 126 Å and length of 625 Å. Upon addition of glucose at a concentration of 100 mg dL^{-1}, the fitted coil diameter (49 Å) and helical pitch (124 Å) did not change considerably, but the nanocoil length increased by ≈4-fold (2790 Å). It is noted that PBAs can form a bisdentate complex with glucose—two PBAs bound to different sites on the same glucose molecule—when in its furanose form,[36–38] though the second binding event is less favorable in part due to a low fraction of glucose in this anomeric form. As no structural changes to the nanocoils were observed upon addition of glucose, apart from their length, it is not anticipated that bisdentate interactions are readily occurring in PBA-MDP assemblies.

The observation of this uncommon nanocoil morphology inspired additional studies using high-resolution structural analysis with cryoEM to uncover the mode of molecular packing. The average power spectrum of aligned nanocoil segments revealed the typical pattern for a helical assembly (Figure 2E). Four layer lines were visible in the power spectrum, which corresponded to four orders of a first layer line at ≈1/(123 Å) arising from a nanocoil pitch of ≈123 Å. This matches well with observations from SAXS. The ring at ≈1/(4.8 Å) in the power spectrum appears to arise from the unpolymerized peptides in the background. Since the spacing of β-strands in a β-sheet is ≈4.8 Å, PBA-MDP likely exists in the background as dimers of two PBA-MDP monomers in either a parallel or antiparallel state. An unambiguous determination of the helical rise of the subunits in the nanocoil was not possible due to the lack of high-resolution information in the average power spectrum. Among many tested possible symmetries, a twist/rise of 15.7°/ 5.1 Å was found to give the best density map, showing separation of β-strands with reasonable density for bulky side chains of the residues (Figure 2F). In this configuration, 24 PBA-MDP dimers are aligned roughly parallel to the helical axis with an axial rise of 5.1 Å to generate a nanocoil with ≈123 Å pitch.

2.3. Impact of Glucose Binding

Results from TEM and SAXS showed limited impact from glucose binding on nanocoil morphology, though the addition of glucose led to an increase in the length and apparent bundling of these nanocoils. As part of the original design rationale, the central region was intended to drive β-sheet hydrogen bonding; though initially envisioned as a fibrilizing domain, the close head-to-tail stacking of the monomers revealed through structural elucidation of the nanocoils by cryoEM could still allow for H-bonding of this domain. Indeed, a β-sheet dimer is likely as the building block for the eventual nanocoil assemblies. Circular

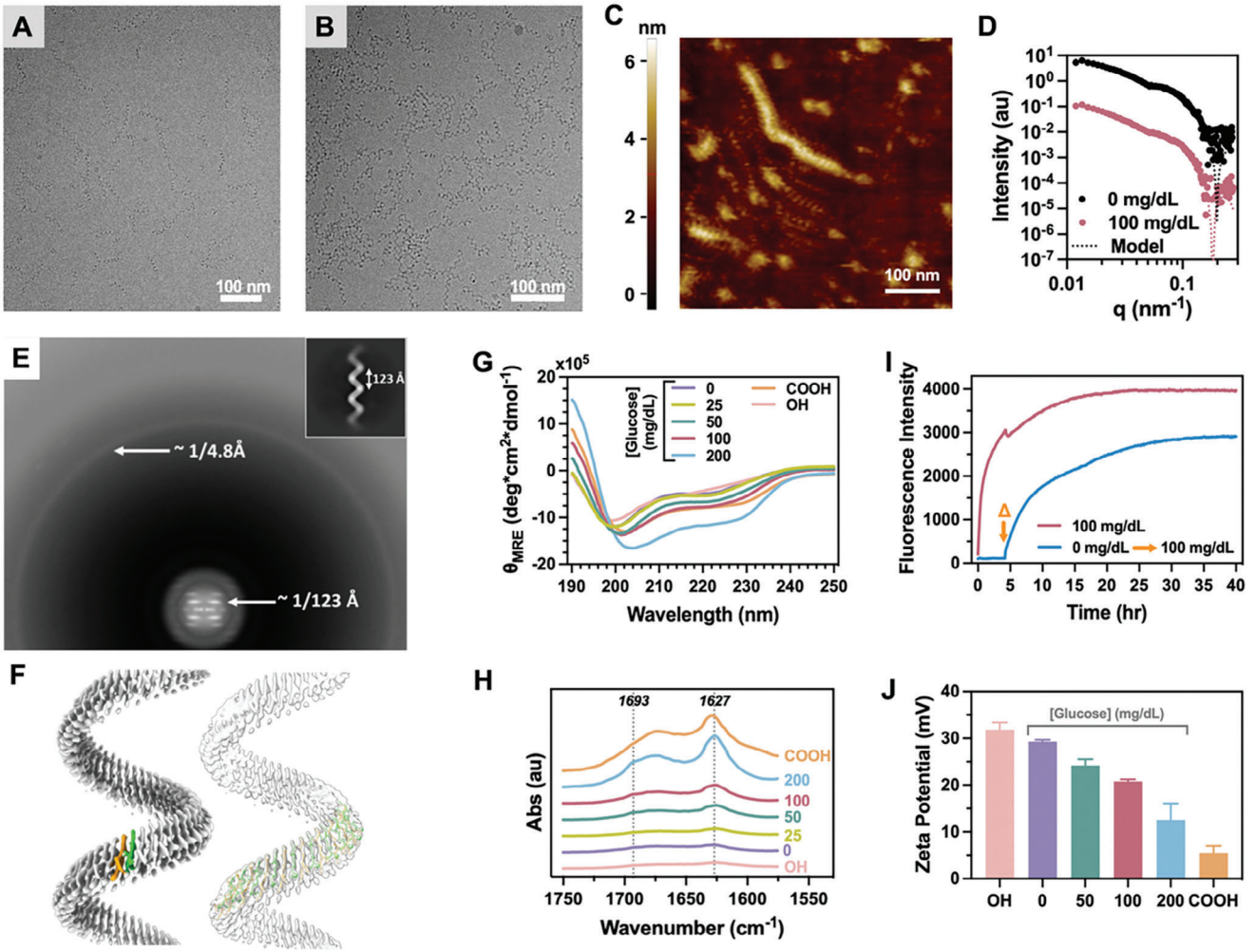

Figure 2. Cryogenic transmission electron microscopy (cryo-TEM) performed on PBA-MDP A) without glucose or B) with 100 mg dL^{-1} glucose. C) Liquid-phase atomic force microscopy (AFM) on PBA-MDP without glucose. D) Small angle X-ray scattering (SAXS) performed on PBA-MDP with or without addition of 100 mg dL^{-1} glucose. E) 2D class average (inset) and power spectrum of vertically aligned nanocoil segments. F) The cryo-EM density map of the nanocoil (left). The density corresponding to a dimer of PBA-MDP (asymmetric unit of helix) are colored orange and green. The atomic model of the nanocoil fitted in to the density map (right). G) Circular dichroism (CD) spectroscopy of PBA-MDP with increasing concentration of glucose, along with controls of COOH-MDP and OH-MDP. H) Fourier transform infrared (FTIR) spectroscopy of PBA-MDP with increasing concentration of glucose, along with controls of COOH-MDP and OH-MDP. The dashed vertical lines denote peaks of interest in the Amide I region of the spectra. I) Thioflavin-T (ThT) fluorescence of PBA-MDP upon immediate addition of glucose (red) or when glucose is added after 4 h of continuous monitoring (blue). J) Zeta potential measurements for PBA-MDP with increasing concentration of glucose, along with controls of COOH-MDP and OH-MDP (n = 3 samples per group, mean ± SD shown).

dichroism (CD) spectroscopy was first performed on PBA-MDP over a range of glucose concentrations from 0 to 200 mg dL^{-1} (Figure 2G). Though these spectra did not conform to the typical canonical secondary structures of a β-sheet, the emergence of a small negative peak at 223 nm and a relatively larger negative peak at 201 nm were generally consistent with predictions for a right-twisted antiparallel β-sheet;[39] red-shifting of these minima as glucose concentration increased suggests glucose acts to increase twisting of these antiparallel interactions. This interpretation of CD data is further supported by the characteristic β-sheet spacing of ≈4.8 Å revealed in structural cryoEM studies. Though TEM and SAXS demonstrate that the nanocoil morphology does not change upon addition of glucose, it is postulated that these glucose-dependent changes in secondary structure present in CD arise from the antiparallel β-sheet dimers observed in the background of cryoEM studies being recruited to participate in nanocoil assemblies when glucose is present. Both control molecules COOH-MDP and OH-MDP generally revealed similar secondary structure signatures by CD, with signal intensity increased for the COOH-MDP variant. It is likewise noted that the inclusion of aromatic amino acids on self-assembling peptides can confound interpretation of CD as a result of π–π^* and n–π^* transitions present specifically in the spectral region of interest here.[40] Given the uncharacteristic nature of these peaks relative to typical self-assembling oligopeptides, Fourier transform infrared spectroscopy (FTIR) was next performed to further characterize stretches in the Amide I region as a means of assessing peptide secondary structure (Figure 2H).

A major peak was observed at 1627 cm^{-1} with a minor peak at 1693 cm^{-1}; these peaks in the Amide I region correspond to those reported for a model peptide that is known to form antiparallel β-sheets.[41] These signatures were enhanced by the addition of glucose, supporting an increased propensity to form antiparallel β-sheets for PBA-MDP in its glucose-bound state. Control molecules demonstrated the impact of prosthetic charge on this β-sheet formation as well, with the uncharged prosthetic of the OH-MDP leading to limited antiparallel β-sheet signal in this region while the charged prosthetic of the COOH-MDP corresponded to a very strong signal. Accordingly, the PBA motif is expected to become increasingly charged as glucose level increases, a known outcome of PBA motifs wherein the equilibrium shifts to the charged tetrahedral boronate in water upon glucose binding.[42] The presence of a negative prosthetic charge at this position, and thus a more neutralized *N*-terminal domain, therefore appears to promote enhanced antiparallel β-sheet formation. However, given microscopy results showing nanocoils from PBA-MDP in both the presence and absence of glucose, the existence of well-ordered antiparallel β-sheet interactions is seemingly not essential to nanocoil formation though may have implications on the overall increase in nanocoil length through internal stabilization. Moreover, the CD signal of an antiparallel β-sheet in all samples irrespective of glucose levels could also arise from H-bonding of PBA-MDP dimers existing in equilibrium with the nanocoil structures that are accentuated in the presence of glucose. Indeed, the likely presence of a background of peptide dimers spaced by ≈4.8 Å revealed in structural cryoEM support this hypothesis.

To further verify the glucose-dependent emergence of β-sheet structures, thioflavin T (ThT) was used (Figure 2I). The fluorescence of this dye increases when embedded in β-sheet-rich domains, offering a means to sense and monitor amyloid structures.[43] When PBA-MDP was prepared in the presence of 100 mg dL^{-1} glucose, ThT fluorescence showed a steady increase over a period of ≈20 h. When PBA-MDP was prepared in the absence of glucose, limited ThT fluorescence was observed. However, when this sample was transferred to 100 mg dL^{-1} glucose at 4 h after preparation, the ThT fluorescence began to increase immediately upon introduction of glucose. Taken together with results from CD and FTIR, these data support a role for glucose binding in triggering increased antiparallel β-sheet ordering in PBA-MDP assemblies. It is worth reiterating that TEM and SAXS data demonstrate the existence of these β-sheet structures is not essential to the formation of the nanocoil assemblies, though a greater antiparallel β-sheet propensity along with recruitment of antiparallel β-sheet dimers to extending nanocoils could underlie the increase in nanocoil length observed by TEM and SAXS in the presence of glucose.

The original design rationale was that glucose binding to the prosthetic PBA motif would stabilize a negative charge on the boronate and make the *N*-terminal end of the molecule net-neutral. Accordingly, Zeta potential was also measured for PBA-MDP as a function of glucose (Figure 2J). At pH 7.4, it is expected that both the arginine and lysine residues would be fully charged, while the boronate would likely exist in both its negatively charged tetrahedral configuration and uncharged trigonal form; the extent to which the neighboring arginine residue lowers the pK_a of this boronate from its nominal value of ≈8.4 is not clear. Thus, the molecule would be expected to be net-positive overall, with the magnitude of its charge state depending on the extent to which the boronate was charged. In the absence of glucose, PBA-MDP had a substantial positive zeta potential of ≈29.3 mV. The magnitude of this positive zeta potential decreased corresponding to an increase in glucose up to 200 mg dL^{-1}, wherein the zeta potential was reduced to ≈12.6 mV. As a control, the uncharged prosthetic of OH-MDP, with a nominal net charge of +2 for the overall molecule, had the most positive zeta potential of ≈31.8 mV. Meanwhile, the negatively charged prosthetic of the COOH-MDP, with a nominal net charge of +1, had the least positive zeta potential of ≈5.5 mV. These data support a gradient in the charge state of the PBA motif on the PBA-MDP, becoming increasingly negative as glucose binding shifts the equilibrium to its tetrahedral configuration. These data likely also support a role for charge screening in the increased nanocoil length and extent of bundling observed in cryoTEM for PBA-MDP as glucose level is increased.

2.4. Glucose-Driven Hydrogelation

When PBA-MDP was prepared at concentrations of 1.5% w/v in the presence of 100 mg dL^{-1} glucose, a self-supporting hydrogel was observed (**Figure 3A**). This observation was further evaluated over a range of glucose concentration from 0 to 200 mg dL^{-1}. Over a period of minutes following preparation, samples with 100 and 200 mg dL^{-1} glucose formed translucent self-supporting hydrogels. Meanwhile, samples prepared at lower glucose levels (0, 25, and 50 mg dL^{-1}) remained translucent but were not able to be inverted to demonstrate self-supporting character. Accordingly, by gross macroscopic inspection using vial inversion, the addition of glucose promotes hydrogelation of solutions of PBA-MDP. To further support these observations for steady gelation upon addition of glucose, a rheological time-course study was next performed (Figure 3B). Samples of PBA-MDP were freshly prepared immediately before measurements at 1.5% w/v in pH 7.4 HEPES buffer and placed onto the rheometer stage. The initial storage modulus (G') and complex viscosity (η^*) were similar in both conditions (G' = ≈23 Pa and η^* = ≈5 Pa s). In the sample prepared with 100 mg dL^{-1} glucose, G' and η^* increased rapidly over the first 10 min to ≈240 Pa and ≈48 Pa s, respectively. Further measurements over the next 35 min demonstrated a plateau in G' = 507 Pa and η^* = 102 Pa s. Comparatively, the PBA-MDP *sol* prepared with no glucose, G' and η^* stayed relatively stable with only a small increase in G' = ≈41.3 Pa and η^* = ≈9 Pa s. These data support a role for glucose in promoting hydrogelation of PBA-MDP, possibly resulting from the overall increase in nanocoil length and extent of bundling that was observed in TEM studies performed in the presence of glucose.

The effect of glucose concentration on gelation was further studied in samples brought to steady-state over 45 min in various glucose concentrations (0, 25, 50, 100, and 200 mg dL^{-1}) prior to rheological measurements. G' and η^* both increased by almost 2 orders of magnitude with an increase in glucose concentration, from G' = 16.7 Pa and η^* = 3.4 Pa s at 0 mg dL^{-1} to G' = 1009.8 Pa and η^* = 203.3 Pa s at 100 mg dL^{-1} (Figure 3C). With the further increase in glucose to 200 mg dL^{-1} glucose, negligible additional increase was observed for G' or η^*. A largeb

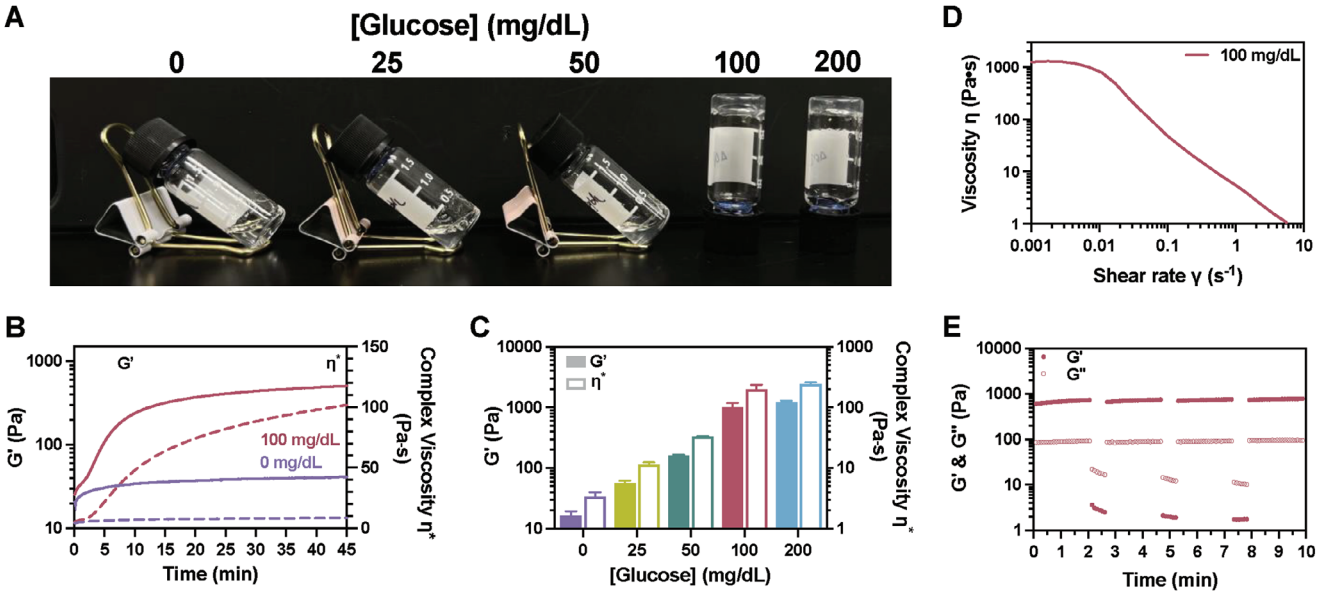

Figure 3. A) Hydrogelation of PBA-MDP as observed by vial inversion under different glucose conditions. B) Evolution of the storage modulus (*G'*, solid, left axis) and complex viscosity (η^*, dashed, right axis) over time following addition of glucose and application onto the rheometer. C) Glucose-dependent changes in the plateau storage modulus (*G'*, solid, left axis) and complex viscosity (η^*, open, right axis), from $n = 2$ samples per group (mean ± SD shown). D) Shear viscosity ramp and E) step-strain cycling from 1% to 100% strain for a PBA-MDP hydrogel prepared in 100 mg dL^{-1} glucose.

increase in *G'* occurred for an increase in glucose level from 50 mg dL^{-1} (*G'* = 165.2 Pa) to 100 mg dL^{-1} (*G'* = 1009.8 Pa); importantly this range in glucose concentration corresponds to a low to normal blood glucose level, suggesting the possibility for function in physiologically relevant conditions. The trends in gelation and viscosity as a function of glucose align with observations from cryoTEM and SAXS pointing to a greater extent of nanocoil bundling and entanglement and longer nanocoil structures upon addition of glucose. These measurements performed on bulk gels aged in vials result in higher measured *G'* values than when gels were aged on the rheometer, likely resulting from being aged in the absence of continuous deformation. COOH-MDP also formed hydrogels at 1.5% w/v; rheology on samples prepared and equilibrated overnight revealed these to be stiffer with a higher complex viscosity (Figure S7, Supporting Information) than PBA-MDP hydrogels, further supporting increased intermolecular interactions and reduced electrostatic repulsion for COOH-MDP that was observed by CD, FTIR, and zeta potential measurements.

Toward injection-relevant applications, the PBA-MDP hydrogel should be shear-thinning and self-healing, allowing it to pass through a needle under shear and immediately reform its gel structure once in situ.[44] A hydrogel prepared in 100 mg dL^{-1} glucose exhibited reduced viscosity of over three orders of magnitude from a "zero-shear" level of ≈1400 Pa s to <1 Pa s at a shear rate of 10 s^{-1} (Figure 3D). Another crucial property of an injectable hydrogel is its ability to self-heal following exposure to high strain. To probe this feature, the PBA-MDP hydrogel prepared with 100 mg dL^{-1} glucose was thus exposed to cyclic strain between 1% and 100% at a constant frequency of 10 rad s^{-1} (Figure 3E). Mechanical properties of the hydrogel recovered immediately after cessation of high strain, a process repeated for multiple cycles.

2.5. Glucose-Responsive Drug Delivery

Evidence for glucose binding-induced formation and stabilization of PBA-MDP nanocoil hydrogels supported their further exploration in the context of glucagon therapy. As an antagonist to insulin, glucagon functions in normal physiology to reverse low blood glucose (hypoglycemia).[45] While exogenous glucagon is only commonly used in the context of emergency rescue, the integration of glucose-responsive therapeutic glucagon delivery may also enable enhanced precision in insulin-centered blood glucose control by mitigating the risks of hypoglycemia.[46] An ideal glucagon delivery approach should thus exhibit release and/or activity inversely related to blood glucose level. As an active glucagon payload, dasiglucagon was selected for its improved solubility and stabilized secondary structure relative to native glucagon.[47] To first monitor release as a function of ambient glucose level, a fluorescent variant (MCA-dasiglucagon)[22] was used. MCA-dasiglucagon alone had rapid release that was effectively independent of glucose (Figure S8, Supporting Information), likely due to the relatively small payload compared to the mesh size of the nanocoil network. Thus, MCA-dasiglucagon was instead co-formulated with protamine, an arginine-rich polypeptide, to increase the hydrodynamic size of the payload and limit its leakage from the hydrogels. Protamine is also used in complex with insulin in the long-used clinical NPH Insulin product.[48] The release profiles of dasiglucagon following its complexation with protamine revealed an inverse glucose dependence (**Figure 4A**). Fitting to a standard first-order model demonstrated decreased rates of release and plateau values when glucose was increased over a range from 0 to 200 mg dL^{-1}. It is noted that the control hydrogel of COOH-MDP exhibited a similar release behavior as the PBA-MDP hydrogel at a glucose concentration of 200 mg dL^{-1} and, when taken together with material characterization data,

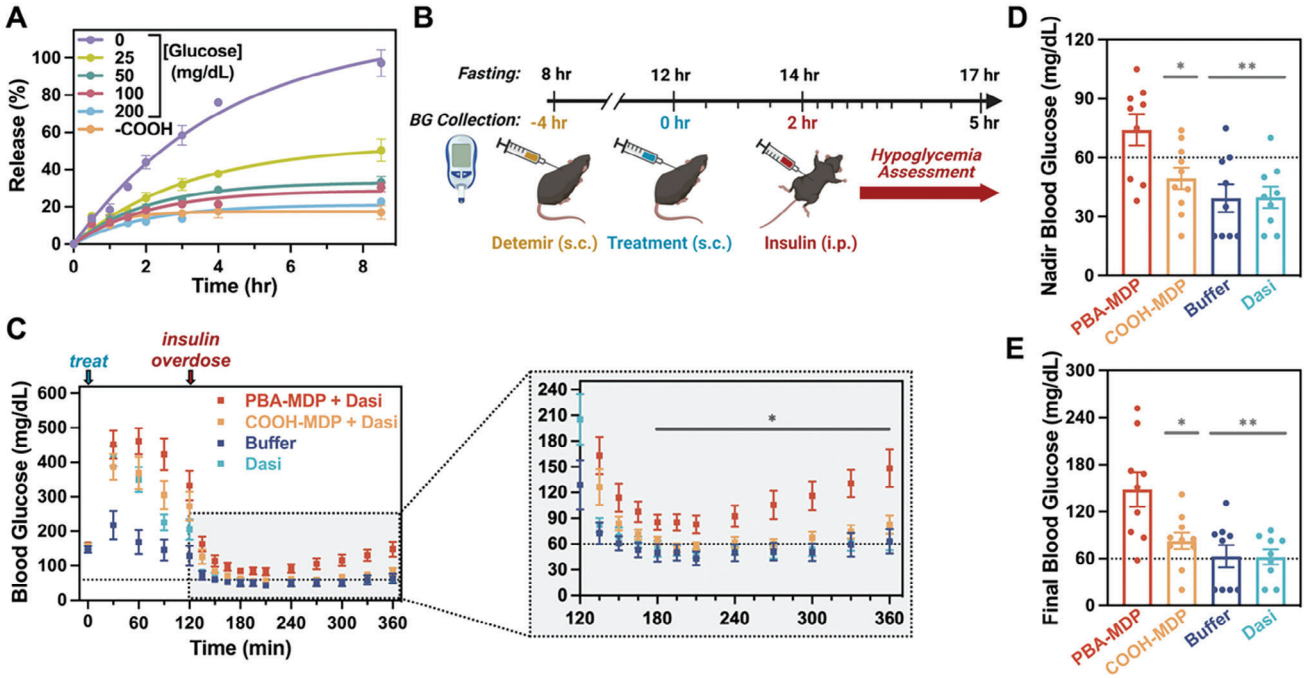

Figure 4. A) Release of encapsulated dasiglucagon from PBA-MDP hydrogels prepared at 100 mg dL^{-1} glucose and incubated in a buffer of varying glucose levels ($n = 3$ samples per group, mean ± SD shown). B) Mouse model for prophylactic glucagon delivery prior to severe hypoglycemia caused by insulin overdose. C) Blood glucose is monitored over time, focusing specifically on the region following insulin overdose (zoomed shaded region). Groups were compared on the basis of D) the lowest (nadir) blood glucose level observed as well as E) the final blood glucose level at 4 h after the insulin overdose. For panel C-E, $n = 9$–10 mice per group, mean ± SEM shown. For panel (C), multiple unpaired *t*-tests were performed at each timepoint, using the Holm–Šídák method to correct for multiple comparisons (* – $P < 0.05$ for PBA-MDP vs. all other groups from 180 min onward). For panels (D–E), a one-way ANOVA was performed with Bonferroni multiple comparisons post-hoc testing (*– $P < 0.05$, ** – $P < 0.01$ for PBA-MDP vs all other groups).

supports a role for glucose binding-induced neutralization of the peptide *N*-terminal domain in nanocoil stabilization, entanglement, and gelation, thereby slowing dasiglucagon release.

Finally, glucose-induced stability and increased retention of dasiglucagon was explored in a previously established model of prophylactic delivery to prevent a subsequent hypoglycemic emergency (Figure 4B).[22] Streptozotocin (STZ) was used to induce diabetes in mice; following a stable hyperglycemic phenotype, mice were fasted overnight and then administered the clinically used Insulin Detemir to induce a state of normoglycemia. Four hours after administering Insulin Detemir ($t = 0$), control mice were treated with either buffer or 0.01 mg dasiglucagon, while experimental groups were administered 0.01 mg dasiglucagon encapsulated in 50 µL hydrogels of either PBA-MDP or COOH-MDP. After two additional hours, mice were overdosed by injection of 3 IU kg^{-1} recombinant human insulin. Blood glucose levels were monitored throughout the procedure (Figure 4C). A threshold for hypoglycemia, set nominally at 60 mg dL^{-1}, was used to monitor the severity of hyperglycemic response following insulin overdose. Among the four groups, the lowest average blood glucose level observed (nadir value, Figure 4D) was above this hypoglycemic threshold for only the mice treated with the PBA-MDP hydrogel containing dasiglucagon (74 ± 8 mg dL^{-1}). The buffer-treated (39 ± 7 mg dL^{-1}) and dasiglucagon-treated (40 ± 5 mg dL^{-1}) groups were both significantly less (P <0.01) than the group treated with the PBA-MDP hydrogel. The lack of function for dasiglucagon administered 2 h prior to insulin overdose is not surprising given the relatively short half-life of the hormone,[49] and also is supported by previous studies in this same model.[22] The glucose-responsive function of the hydrogel was further supported by the performance of the COOH-MDP (49 ± 10 mg dL^{-1}), which resulted in a nadir value significantly lower ($P < 0.05$) than PBA-MDP and illustrates the function to be expected from glucose-independent controlled release. In addition to a prevention of low blood glucose levels, the PBA-MDP hydrogel treatment offered protection against onset of severe hypoglycemia; there were no overdose-related deaths in the PBA-MDP group (0/9) compared to groups treated with the COOH-MDP hydrogel (1/10), buffer (4/9), and dasiglucagon (2/9). The recovery from hypoglycemia was also evaluated at the endpoint of the study (Figure 4E). Mice treated with PBA-MDP hydrogel demonstrated significantly better recovery (148 ± 22 mg dL^{-1}) than mice treated with COOH-MDP hydrogel (83 ± 11 mg dL^{-1}, $_p < 0.05$), buffer (63 ± 14 mg dL^{-1}, $P < 0.01$), and dasiglucagon alone (62 ± 10 mg dL^{-1}, $P < 0.01$).

Accordingly, the glucose-directed retention and release of dasiglucagon from within the PBA-MDP hydrogels offered advantages as a prophylactic (protective) measure against a subsequent sudden hypoglycemic episode brought on by insulin overdose. The performance of this approach to deliver dasiglucagon is likewise comparable in this same model to an orthogonal

approach that used enzymatic actuation by the glucose oxidase enzyme to endow self-assembled peptide hydrogels with glucose-driven stability and afford dasiglucagon release under states of low glucose.[22] The xenogeneic origin of glucose oxidase, along with its toxic hydrogen peroxide byproduct,[21] may limit the therapeutic utility of this prior work in the therapeutic context of a routine glucagon prophylactic. By comparison, the approach presented here using a single-component system of glucose-binding nanocoils may offer distinct advantages. Namely, the current system does not require a xenogeneic enzyme with immunogenic risk, nor does it entail a toxic H_2O_2 byproduct, instead achieving its function through a discrete small molecule assembly process including a synthetic PBA glucose binder. Certain drawbacks of this prior system,[22] including undesirable glucagon leakage after injection and lower responsibility than would be desirable in emergency-use contexts, remain challenges in the PBA-MDP platform as well.

3. Conclusion

Herein, a multidomain peptide bearing a terminal PBA motif is shown to self-assemble into an uncommon nanocoil morphology. These peptide nanocoils seemingly arise from antiparallel dimers of PBA-MDP that further organize into nanocoils with peptides aligned parallel to the *z*-axis of the nanocoil. Advanced structural techniques leveraging cryoEM further elucidate the likely molecular arrangement in these nanocoils. The necessity of including negative charge-bearing groups at the terminal PBA region is supported by a control molecule with a carboxylic acid in place of the boronate. Meanwhile, a neutral hydroxyl modification does not achieve a similar nanocoil morphology. The presence and amount of glucose dictates an increasingly negative charge by shifting the boronate equilibrium from its uncharged trigonal form to its anionic tetrahedral form, with direct implications on driving PBA-MDP nanocoil elongation and entanglements and an enhanced extent of antiparallel β-sheet formation. Glucose further leads to the formation of self-supporting hydrogels, with stiffness directed by glucose levels spanning a physiologically relevant range. The glucose-stabilized nature of these hydrogels encouraged further investigation for their encapsulation and controlled release of dasiglucagon, a therapeutic remedy for low blood glucose. Indeed, release from PBA-MDP hydrogels is inversely related to glucose level, offering a means of potentially delivering glucagon that is responsive to the needs of low blood glucose levels. Studies of dasiglucagon delivery performed in a mouse model of prophylactic delivery followed by insulin overdose point to enhanced protection against hypoglycemia for delivery using PBA-MDP hydrogels. As such, the uncommon nanocoil morphology here enables formation of hydrogels for functional glucose-responsive therapeutic delivery. Though future manifestations should seek more rapid therapeutic response with limited dasiglucagon leakage under states of normoglycemia, and address the lack of glucose specificity of the PBA motif used,[26] this general approach offers practical improvements over previously reported peptide assemblies that relied on actuation from an xenogeneic enzyme to achieve their function.[22]

4. Experimental Section

Detailed experimental methods are found in the Supporting Information. In brief, all peptides and dasiglucagon were synthesized by solid phase peptide synthesis and purified using HPLC. MDP samples were first prepared by dissolving in DI water at 3% w/v and then diluted 1:1 in 2x HEPES buffer to reach a final concentration of 1.5% w/v in 1x buffer, with glucose concentration of the buffer varied accordingly. Gelation was studied using rheology on samples prepared at this initial concentration of 1.5% w/v. FTIR was performed on dried samples, CD was performed on samples diluted 10x immediately before measurement, SAXS was performed on samples prepared at 1.5% w/v, and AFM and zeta potential were performed on MDP solutions diluted to 0.2% w/v prior to measurements. In vitro encapsulation and release studies used a fluorescently labeled (MCA) dasiglucagon variant, prepared as previously described.[22] All animal studies were performed at the University of Notre Dame, following methods that were previously reported,[22] and according to a protocol approved by the Notre Dame Animal Care and Use Committee (Assurance of Compliance #A3093-01). Statistical analysis was performed using GraphPad Prism (V9.5.1), with error presentation (SD or SEM) and statistical testing methods (*t*-tests, ANOVA, post-hoc testing) performed as noted in the captions of each figure.

Supporting Information

Supporting Information is available from the Wiley Online Library or from the author.

Acknowledgements

S.Y. and Z.Y. contributed equally to this work. M.J.W. gratefully acknowledged funding support for this work from the American Diabetes Association Pathway Award (No. 1-19-ACE-31), The Helmsley Charitable Trust (No. 2019PG-T1D016), the Juvenile Diabetes Research Foundation (No. 5-CDA-2020-947-A-N).

Conflict of Interest

The authors declare no conflict of interest.

Data Availability Statement

The data that support the findings of this study are available from the corresponding author upon reasonable request.

Keywords

drug delivery, hydrogel, nanotechnology, supramolecular chemistry

Received: October 31, 2023
Revised: December 11, 2023
Published online:

[1] G. M. Whitesides, B. Grzybowski, *Science* **2002**, *295*, 2418.
[2] I. W. Hamley, *Biomacromolecules* **2019**, *20*, 1829.
[3] E. D. Korn, M.-F. Carlier, D. Pantaloni, *Science* **1987**, *238*, 638.
[4] H.-W. Wang, E. Nogales, *Nature* **2005**, *435*, 911.
[5] A. Sorrenti, J. Leira-Iglesias, A. J. Markvoort, T. F. A. De Greef, T. M. Hermans, *Chem. Soc. Rev.* **2017**, *46*, 5476.

[6] J. Deng, A. Walther, *Adv. Mater.* **2020**, *32*, 2002629.
[7] A. Mishra, D. B. Korlepara, M. Kumar, A. Jain, N. Jonnalagadda, K. K. Bejagam, S. Balasubramanian, S. J. George, *Nat. Commun.* **2018**, *9*, 1295.
[8] A. Mishra, S. Dhiman, S. J. George, *Angew. Chem., Int. Ed. Eng.* **2021**, *60*, 2740.
[9] K. Das, L. Gabrielli, L. J. Prins, *Angew. Chem., Int. Ed. Eng.* **2021**, *60*, 20120.
[10] H. Cui, M. J. Webber, S. I. Stupp, *Biopolymers* **2010**, *94*, 1.
[11] M. J. Sis, M. J. Webber, *Trends Pharmacol. Sci.* **2019**, *40*, 747.
[12] R. V. Ulijn, A. M. Smith, *Chem. Soc. Rev.* **2008**, *37*, 664.
[13] J. Wang, K. Liu, R. Xing, X. Yan, *Chem. Soc. Rev.* **2016**, *45*, 5589.
[14] D. W. P. M. Löwik, E. H. P. Leunissen, M. Van Den Heuvel, M. B. Hansen, J. C. M. Van Hest, *Chem. Soc. Rev.* **2010**, *39*, 3394.
[15] Y. Gao, Z. Yang, Y. Kuang, M.-L. Ma, J. Li, F. Zhao, B. Xu, *Biopolymers* **2010**, *94*, 19.
[16] R. J. Mart, R. D. Osborne, M. M. Stevens, R. V. Ulijn, *Soft Matter* **2006**, *2*, 822.
[17] M. J. Webber, *Bioeng. Transl. Med.* **2016**, *1*, 252.
[18] M. Tena-Solsona, B. Rieß, R. K. Grötsch, F. C. Löhrer, C. Wanzke, B. Käsdorf, A. R. Bausch, P. Müller-Buschbaum, O. Lieleg, J. Boekhoven, *Nat. Commun.* **2017**, *8*, 15895.
[19] A. Sorrenti, J. Leira-Iglesias, A. Sato, T. M. Hermans, *Nat. Commun.* **2017**, *8*, 15899.
[20] M. A. Vandenberg, M. J. Webber, *Adv. Healthcare Mater.* **2019**, *8*, 1801466.
[21] Y. Xiang, B. Su, D. Liu, M. J. Webber, *Adv. Ther.* **2023**, 2300127, https://doi.org/10.1002/adtp.202300127.
[22] S. Yu, S. Xian, Z. Ye, I. Pramudya, M. J. Webber, *J. Am. Chem. Soc.* **2021**, *143*, 12578.
[23] B. Marco-Dufort, M. W. Tibbitt, *Mater. Today Chem.* **2019**, *12*, 16.
[24] W. L. A. Brooks, B. S. Sumerlin, *Chem. Rev.* **2016**, *116*, 1375.
[25] R. Ma, L. Shi, *Polym. Chem.* **2014**, *5*, 1503.
[26] Y. Xiang, S. Xian, R. C. Ollier, S. Yu, B. Su, I. Pramudya, M. J. Webber, *J. Controlled Release* **2022**, *348*, 601.
[27] H. Dong, S. E. Paramonov, L. Aulisa, E. L. Bakota, J. D. Hartgerink, *J. Am. Chem. Soc.* **2007**, *129*, 12468.
[28] S. Kitano, I. Hisamitsu, Y. Koyama, K. Kataoka, T. Okano, Y. Sakurai, *Polym. Adv. Technol.* **1991**, *2*, 261.
[29] J. Jover, R. Bosque, J. Sales, *QSAR Comb. Sci.* **2008**, *27*, 563.
[30] Y. Li, M. Kim, T. H. Pial, Y. Lin, H. Cui, M. Olvera De La Cruz, *J. Phys. Chem. B* **2023**, *127*, 8176.
[31] C. Tang, A. M. Smith, R. F. Collins, R. V. Ulijn, A. Saiani, *Langmuir* **2009**, *25*, 9447.
[32] Y. Wang, K. Kaur, S. J. Scannelli, R. Bitton, J. B. Matson, *J. Am. Chem. Soc.* **2018**, *140*, 14945.
[33] Y. Wang, Y. An, Y. Shmidov, R. Bitton, S. A. Deshmukh, J. B. Matson, *Mater. Chem. Front.* **2020**, *4*, 3022.
[34] Z. Li, S. Y. Joshi, Y. Wang, S. A. Deshmukh, J. B. Matson, *Angew. Chem., Int. Ed. Eng.* **2023**, *62*, 202303755.
[35] D. V. Lebedev, D. M. Baitin, A. K. Islamov, A. I. Kuklin, V. K. Shalguev, V. A. Lanzov, V. V. Isaev-Ivanov, *FEBS Lett.* **2003**, *537*, 182.
[36] A. M. Horgan, A. J. Marshall, S. J. Kew, K. E. S. Dean, C. D. Creasey, S. Kabilan, *Biosens. Bioelectron.* **2006**, *21*, 1838.
[37] C. Ancla, V. Lapeyre, I. Gosse, B. Catargi, V. Ravaine, *Langmuir* **2011**, *27*, 12693.
[38] J. C. Norrild, H. Eggert, *J. Am. Chem. Soc.* **1995**, *117*, 1479.
[39] A. Micsonai, F. Wien, L. Kernya, Y.-H. Lee, Y. Goto, M. Réfrégiers, J. Kardos, *Proc. Natl. Acad. Sci. USA* **2015**, *112*, E3095.
[40] M. J. Krysmann, V. Castelletto, I. W. Hamley, *Soft Matter* **2007**, *3*, 1401.
[41] E. Cerf, R. Sarroukh, S. Tamamizu-Kato, L. Breydo, S. Derclaye, Y. F. Dufrêne, V. Narayanaswami, E. Goormaghtigh, J.-M. Ruysschaert, V. Raussens, *Biochem. J.* **2009**, *421*, 415.
[42] A. Matsumoto, S. Ikeda, A. Harada, K. Kataoka, *Biomacromolecules* **2003**, *4*, 1410.
[43] M. Biancalana, K. Makabe, A. Koide, S. Koide, *J. Mol. Biol.* **2009**, *385*, 1052.
[44] J. K. Sahoo, M. A. Vandenberg, M. J. Webber, *Adv. Drug Delivery Rev.* **2018**, *127*, 185.
[45] J. R. Chabenne, P. A. Mroz, J. P. Mayer, R. D. Dimarchi, *J. Med. Chem.* **2020**, *63*, 3447.
[46] Z. Wang, J. Wang, H. Li, J. Yu, G. Chen, A. R. Kahkoska, V. Wu, Y. Zeng, D. Wen, J. R. Miedema, J. B. Buse, Z. Gu, *Proc. Natl. Acad. Sci. USA* **2020**, *117*, 29512.
[47] U. Hövelmann, B. V. Bysted, U. Mouritzen, F. Macchi, D. Lamers, B. Kronshage, D. V. Møller, T. Heise, *Diabetes Care* **2018**, *41*, 531.
[48] J. Pettus, T. Santos Cavaiola, W. V. Tamborlane, S. Edelman, *Diabetes Metab. Res. Rev.* **2016**, *32*, 478.
[49] A. E. Pontiroli, A. Calderara, M. G. Perfetti, S. R. Bareggi, *Eur. J. Clin. Pharmacol.* **1993**, *45*, 555.